RESEARCH ARTICLE

The Functional Characterization of Bat and Human P[3] Rotavirus VP8*s

Dandi Li[1,2] · Mengxuan Wang[1,2] · Tongyao Mao[1,2] · Mingwen Wang[1,2] · Qing Zhang[1,2] · Hong Wang[1,2] · Lili Pang[1,2] · Xiaoman Sun[1,2] · Zhaojun Duan[1,2]

Abstract

P[3] rotavirus (RV) has been identified in many species, including human, simian, dog, and bat. Several glycans, including sialic acid, histo-blood group antigens (HBGAs) are reported as RV attachment factors. The glycan binding specificity of different P[3] RV VP8*s were investigated in this study. Human HCR3A and dog P[3] RV VP8*s recognized glycans with terminal sialic acid and hemagglutinated the red blood cells, while bat P[3] VP8* showed neither binding to glycans nor hemagglutination. However, the bat P[3] VP8* mutant of C189Y obtained the ability to hemagglutinate the red blood cells, while human P[3] HCR3A/M2-102 mutants of Y189C lost the ability. Sequence alignment and structural analysis indicated that residue 189 played an important role in the ligand recognition and may contribute to the cross-species transmission. Structural superimposition exhibited that bat P[3] VP8* model was quite different from the simian P[3] Rhesus rotavirus (RRV) P[3] VP8*, indicating that bat P[3] RV was relatively distinct and partially contributed to the no binding to tested glycans. These results promote our understanding of P[3] VP8*/glycans interactions and the potential transmission of bat/ human P[3] RVs, offering more insight into the RV infection and prevalence.

Keywords Bat rotavirus · P[3] VP8* · Glycan binding specificity · Hemagglutination · Sialic acid

Introduction

Rotavirus (RV) is a major pathogen leading to the acute viral gastroenteritis in young children and animals. RV genome contains 11 double stranded RNA fragments, encoding 12 proteins, including 6 structural and 6 non-structural proteins (Estes 2013). Based on VP6, RVs can be divided into ten different species by now, including A-H, one tentative species I, and a candidate species J (Banyai et al. 2017). The RV particle consists of three capsid layers. Two major surface proteins, VP7 and VP4, formed the

Dandi Li and Mengxuan Wang have contributed equally to this work.

✉ Xiaoman Sun
  sunxiaoman88@163.com

✉ Zhaojun Duan
  zhaojund@126.com

[1] National Health Commission Key Laboratory for Medical Virology and Viral Diseases, Beijing 102206, China

[2] National Institute for Viral Disease Control and Prevention, China CDC, Beijing 102206, China

outer most layer and played an important role in inducing neutralizing antibodies and protective immunity. VP7 and VP4 defined the RV G and P genotypes, respectively (Matthijnssens et al. 2011). The group A RVs are diverse and has been identified 51 P genotypes so far (https://rega.kuleuven.be/cev/viralmetagenomics/virus-classification/7th-RCWG-meeting). VP4 can be cleaved by trypsin into two fragments, VP5* and VP8* (Fiore et al. 1991). VP8* located at the distal part of the VP4 spike and was reported to be essential in the glycan recognition and cell attachment (Dormitzer et al. 2002a).

RVs were identified in many species, including human, porcine, bovine, dog and birds. Bats, the reservoirs of many viruses, were also identified to harbor the RVs (He et al. 2013). The genetic analysis of bat RVs indicated the bat-to-human transmission and reassortment (He et al. 2017; Komoto et al. 2020). The cross-species transmission of RVs has been reported in several RV genotypes, including P[6], P[3] RVs that were reported in both human and animal infections (Nyaga et al. 2018; Okitsu et al. 2018). P[3] RVs were identified in various species, including human, simian, dog, and bat (Tsugawa and Hoshino 2008;

He *et al.* 2013; Sasaki *et al.* 2016). Bat P[3] LZHP2 was identified in an insectivorous bat and shared high nucleotide identity with the unique human strain M2-102 that was suggested to originate from a bat RV as a result of cross-species transmission and was divergent from other human RV strains (Dong *et al.* 2016; He *et al.* 2017). Human HCR3A was supposed to be of dog origin (Tsugawa and Hoshino 2008). The molecular mechanism of the prevalence of these P[3] RVs remained elusive.

Attachment to the cell receptors is crucial for the virus infection and transmission. The illustration of the interactions between virus and ligand provided the basis for understanding host tropism, host adaptation, and zoonosis. Previous studies have shown that some animal RVs recognize sialic acid-containing glycoconjugates and are neuraminidase sensitive (Ciarlet and Estes 1999; Isa *et al.* 2006). Some animal RV VP8*s, including P[1] bovine Nebraska calf diarrhea virus, P[2] simian SA11, P[7] porcine CRW-8 were reported to interact with terminal sialic acids on the cell surface glycans (Ciarlet and Estes 1999). The simian P[3] Rhesus rotavirus (RRV) VP8* recognized N-acetylneuraminic acid (Neu5Ac) and the crystal structure of RRV VP8* in complex with Neu5Ac has also been determined (Dormitzer *et al.* 2002b). The glycan binding site located at one corner of the two beta-sheets. CRW-8 P[7] VP8* was found to bind the sialic acid using the same glycan binding site as that of RRV P[3] (Blanchard *et al.* 2007).

Though the interaction between RRV P[3] and sialic acid has been reported, the glycan binding specificities of the P[3] RVs of other species is not clear yet, especially the bat P[3] RVs. Here, the functional features of bat, human, and dog P[3] RVs were investigated, which deepened the understanding of P[3] RV prevalence and transmission from animals to human.

Materials and Methods

Protein Expression and Purification

The full VP8* fragments (residues 1–231 amino acids) of human HCR3A (Genebank: EU708904), 12,638 (Genebank: LC340022), M2-102 (Genebank: KU597745), dog RV198-95 (Genebank: HQ661137), and bat LZHP2 (Genebank: KX814943) were synthesized by Genewiz company (Suzhou, China) and cloned into pGEX6P-1 with an N-terminal GST tag. The GST-fusion proteins were expressed in *E.coli* and induced with isopropyl-β-D-thiogalactopyranoside (IPTG) at a final concentration of 0.4 mmol/L at 22 °C for 16 h. The recombinant proteins were purified as previously reported (Ma *et al.* 2015; Sun *et al.* 2018). Briefly, the bacteria were collected and resuspended, followed by ultrasonication. The supernatant of the bacterial lysates was filtered through a 0.22 μm membrane (Millipore) and then loaded onto the glutathione sepharose (GE Healthcare Life Sciences). The column was washed with PBS five times. Then the protein of interest was eluted with buffer of 50 mmol/L Tris–HCl, 10 mmol/L reduced glutathione, pH 8.0. The eluted proteins were concentrated and the buffer was changed to PBS. The protein concentration was determined using the BCA kit (BD Biosciences). Bat P[3] mutant of C189Y and human M2-102/HCR3A mutant of Y189C were cloned using the site-directed point mutation. The mutant proteins were expressed and purified as described above. The eluted proteins were analyzed by sodium dodecyl sulfate-polyacrylamide gel electrophoresis (SDS-PAGE).

Oligosaccharide Binding Assay

Enzyme-linked immunosorbent assay (ELISA)-based oligosaccharide binding assays were conducted as previously described (Sun *et al.* 2020). The GST-VP8* fusion proteins were coated onto microtiter plates at 20 μg per well with incubation at 4 °C overnight. Following blockage with 5% nonfat milk, synthetic oligosaccharides conjugated with polyacrylamide (PAA) and biotin were added at 0.2 μg per well. The following oligosaccharides were used in this study: Neu5Ac, Neu5Gc, Neu5Acα2-3Gal, Neu5Acα2-6Gal, siaLea, siaLex, siaLec, Neu5Acα2-3Galβ1-4GlcNAc (3'SLN), A/B disaccharides, H1, H2, lea, lex, leb, ley, mucin core 1–mucin core 6, and core 8 (GlycoTech, USA). Then, horseradish peroxidase (HRP)-conjugated streptavidin (Abcam) was added at 0.1 μg per well. For each step, the plates were incubated at 37 °C for 1 h, and washed five times with 0.5% PBS-Tween 20 buffer between steps. The color reactions were developed using a 3,3',5,5'-tetramethylbenzidine (TMB) kit (BD Biosciences). The absorbance of 450 nm was measured.

Glycan Microarray Screening Analysis

Glycan ligand screening for human M2-102 and bat LZHP2 P[3] VP8*-GST fusion proteins were performed by the Protein-Glycan Interaction Core of the Consortium for Functional Glycomics (CFG) (http://www.functionalgly comics.org/) against a library containing 600 glycans. The identities of all glycans in Version 5.3 of the array are available at http://www.functionalglycomics.org/static/con sortium/resources/resourcecoreh8.shtml. The recombinant GST-VP8* protein was used at protein concentrations of 5 μg/mL and 50 μg/mL, respectively. The bound GST-VP8* proteins were detected using a fluorescence-labeled anti-GST monoclonal antibody (Sigma). Fluorescence was measured and quantified by a microarray scanner and relative fluorescent unit (RFU) for binding to each glycan was calculated (Cholleti *et al.* 2012).

Biolayer Interometry (BLI) Analysis

The interactions between P[3] VP8*s and different oligosaccharides were further analyzed using Octet RED96 (ForteBio., USA). Oligosaccharides with PAA-biotin tag (10 μg/mL) (Neu5Ac, Neu5Gc, Neu5Acα2-3Galβ1-4GlcNA(3'SLN), Neu5Acα2-6Gal, H1, H2, H3, Neu5Acβ2-6(Galβ1-3)GalNAc, B disaccharide, A disaccharide, B tetrasaccharide, core1, core2, core8, siaLea, siaLex, siaLec, lea, leb, lex, ley) were immobilized on the streptavidin-biosensor. The P[3] VP8* proteins (human HCR3A, M2-102, bat LZHP2) were diluted at 10 μmol/L with PBST buffer (PBS with 0.02% Tween-20, 0.5% BSA) and added to the 96-well microplate. The VP8* proteins were injected and binding responses were measured. The apparent equilibrium dissociation constants for VP8* and oligosaccharides were calculated using Octet analyzing software.

Hemagglutination

The GST-VP8* proteins were twofold serially diluted with a starting concentration of 2 mg/mL using PBS buffer and added to 96-well V-bottom plates (Costar) with 50 μL per well. Animal red blood cells (RBCs) (Gelaidisi, Beijing) of porcine, rabbit, bovine, chicken, lamb, and human RBCs (A, B, O types, donated by lab colleagues) were diluted to 1% with PBS. Written informed consents were signed by the colleagues. Authorization for the sampling of human and animal blood was obtained. Then 50 μL of RBC was added to each well. Agglutination was determined after incubation at 25°C for 1 h.

Homology Modeling and Structural Analysis

A homology model of bat P[3] VP8* was constructed based on the structure of RRV P[3]VP8* (PDB identifier [ID] 1KQR) by SWISS-MODEL automated protein structure homology modeling server (http://swissmodel.expasy.org/). The structural superimposition and analysis were performed using pymol (https://pymol.org/2/). The cartoon and surface models of VP8* were shown. The electrostatic potential presentation was calculated with the pymol software.

Results

VP8* Protein Expression and Purification

P[3] VP8*s of human (HCR3A, 12,638, M2-102), dog (RV198-95), and bat (LZHP2) were expressed in a soluble form with an N-terminal GST tag. The GST-VP8* proteins were purified via affinity chromatography and the

molecular weight were about 52 kDa with free GST protein of 26 kDa (Fig. 1).

P[3] VP8*s Recognized Glycans with Different Patterns

VP8* proteins were applied to the ELISA to investigate the binding to synthetic oligosaccharides. Human HCR3A, 12,638, and dog RV198-95 P[3] VP8*s exhibited binding to glycans with sialic acid, such as Neu5Acα2-3Gal, Neu5Acα2-6Gal, and 3'SLN (Fig. 2). Human M2-102 and bat LZHP2 P[3] VP8*s showed no observed binding to the tested glycans.

According to the glycan microarray assay, human M2-102 and bat LZHP2 P[3] VP8* exhibited no specific binding to the tested 600 glycans including glycans with sialic acid (Fig. 3). Relative Fluorescent Units (RFUs) indicated the binding intensity. The Human M2-102 and bat LZHP2 P[3] VP8* did not showed high RFU value to these glycans (Fig. 3). For the glycan 117, the RFUs were almost the same for different concentrations and different kinds of proteins. It is suggested that the binding is regarded to be non-specific.
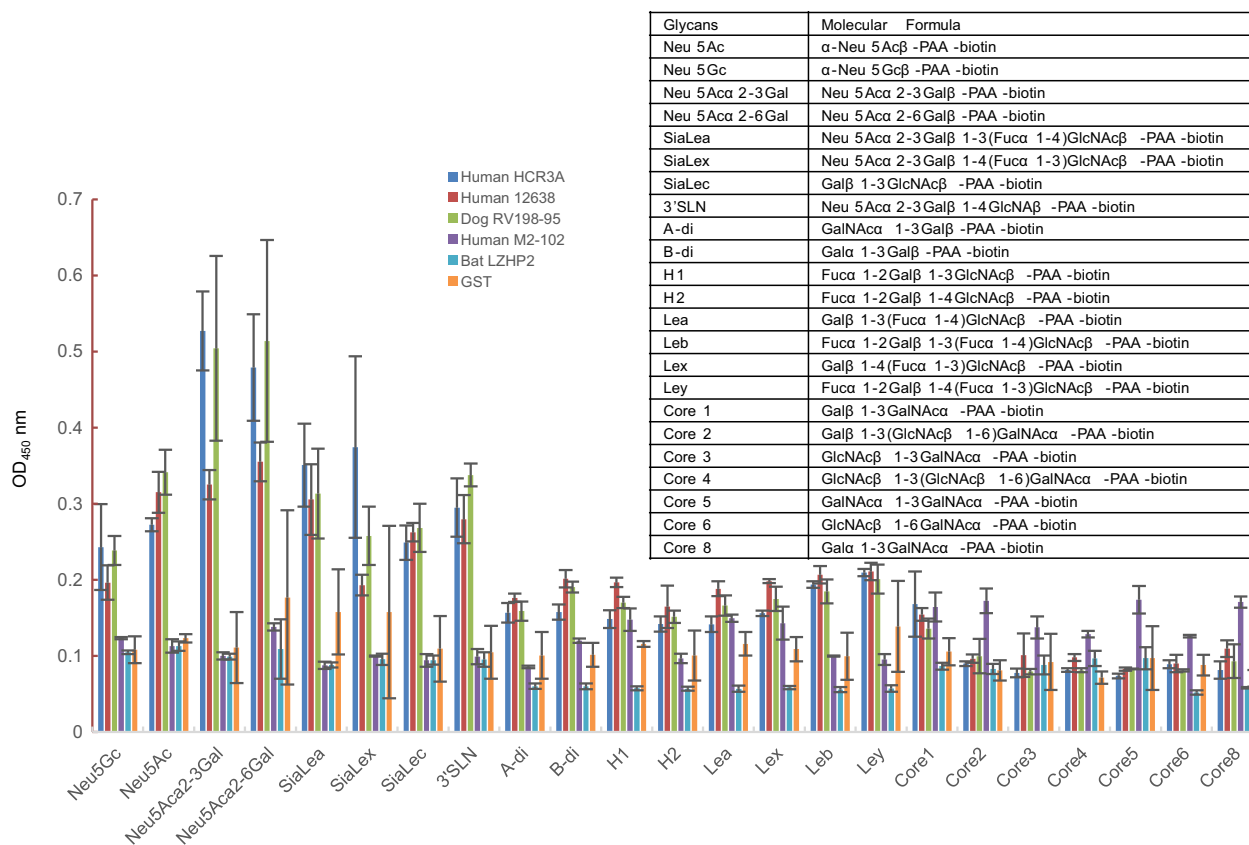
To test the interactions between P[3] VP8*s and different glycans, the biolayer interferometry (BLI) assay was performed using the Octet RED96. The results showed that human HCR3A VP8* specifically recognized glycans with sialic acid, including Neu5Ac, 3'SLN, Neu5Acα2-6Gal, siaLec, siaLea, siaLex (Fig. 4), while P[3] VP8*s of human M2-102 and bat LZHP2 did not recognize any tested glycans.

Hemagglutination of P[3] VP8*s and Mutants

Hemagglutination was performed to explore the interaction between VP8* and the red blood cells. Human
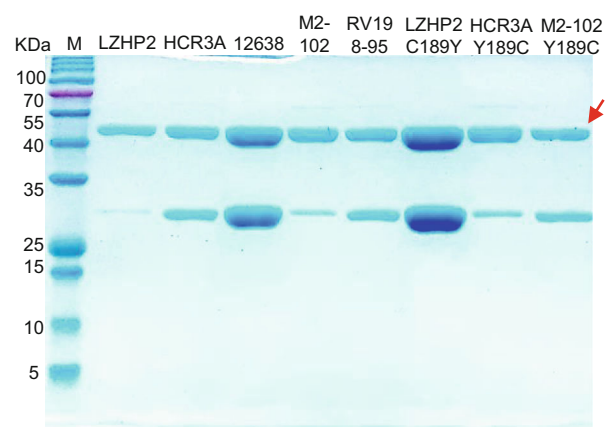
Fig. 1 SDS-PAGE of bat LZHP2 P[3], human HCR3A, 12,638, M2-102 P[3], dog RV198-95 P[3], bat P[3] LZHP2 C189Y, human HCR3A Y189C, human M2-102 Y189C VP8* proteins. The molecular weight of GST-VP8* protein is ~ 52 kDa. The 26 kDa band indicates the free GST protein. The red arrow refers to the protein of interest.

Glycans	Molecular Formula
Neu 5Ac	α-Neu 5Acβ -PAA -biotin
Neu 5Gc	α-Neu 5Gcβ -PAA -biotin
Neu 5Acα 2-3 Gal	Neu 5Acα 2-3 Galβ -PAA -biotin
Neu 5Acα 2-6 Gal	Neu 5Acα 2-6 Galβ -PAA -biotin
SiaLea	Neu 5Acα 2-3 Galβ 1-3 (Fucα 1-4) GlcNAcβ -PAA -biotin
SiaLex	Neu 5Acα 2-3 Galβ 1-4 (Fucα 1-3) GlcNAcβ -PAA -biotin
SiaLec	Galβ 1-3 GlcNAcβ -PAA -biotin
3'SLN	Neu 5Acα 2-3 Galβ 1-4 GlcNAβ -PAA -biotin
A-di	GalNAcα 1-3 Galβ -PAA -biotin
B-di	Galα 1-3 Galβ -PAA -biotin
H1	Fucα 1-2 Galβ 1-3 GlcNAcβ -PAA -biotin
H2	Fucα 1-2 Galβ 1-4 GlcNAcβ -PAA -biotin
Lea	Galβ 1-3 (Fucα 1-4) GlcNAcβ -PAA -biotin
Leb	Fucα 1-2 Galβ 1-3 (Fucα 1-4) GlcNAcβ -PAA -biotin
Lex	Galβ 1-4 (Fucα 1-3) GlcNAcβ -PAA -biotin
Ley	Fucα 1-2 Galβ 1-4 (Fucα 1-3) GlcNAcβ -PAA -biotin
Core 1	Galβ 1-3 GalNAcα -PAA -biotin
Core 2	Galβ 1-3 (GlcNAcβ 1-6) GalNAcα -PAA -biotin
Core 3	GlcNAcβ 1-3 GalNAcα -PAA -biotin
Core 4	GlcNAcβ 1-3 (GlcNAcβ 1-6) GalNAcα -PAA -biotin
Core 5	GalNAcα 1-3 GalNAcα -PAA -biotin
Core 6	GlcNAcβ 1-6 GalNAcα -PAA -biotin
Core 8	Galα 1-3 GalNAcα -PAA -biotin

Fig. 2 The glycan binding specificities of P[3] RV VP8*s. PAA-biotin oligosaccharides such as Neu5Ac, Neu5Gc, Neu5Acα2-3Gal, Neu5Acα2-6Gal, siaLea, siaLex, siaLec, Neu5Acα2-3Galβ1- 4GlcNAc (3'SLN), Neu5Acβ2-6(Galβ1-3)GalNAc were included. The absorption at OD_{450} nm was detected. The molecular formula of these glycans were listed in the table.

HCR3A,12,638, M2-102, and dog RV198-95 P[3] VP8*s hemagglutinated the red blood cells of porcine, chicken, rabbit, bovine, lamb, human A, B, O types (Fig. 5). But bat LZHP2 P[3] VP8*s did not hemagglutinate any cells.

It is noted that the VP8*s with Y189 could hemagglutinate the red blood cells. In order to test the function of residue 189, we constructed the mutants of bat LZHP2 P[3] C189Y, human HCR3A Y189C and M2-102 Y189C. Bat P[3] C189Y could hemagglutinate the red blood cells, whereas human HCR3A P[3] Y189C and M2-102 Y189C showed no hemagglutination (Fig. 5).

Sequence Alignment of P[3] VP8*s of Different Origins

Sequence alignment showed that bat LZHP2 P[3] VP8*s possessed various amino acids with the sequence identity of 84.4%, 84.4%, 97.4%, 84.0% compared to VP8*s of human HCR3A, 12,638, M2-102, dog RV198-95 P[3], respectively. The residues involved in the glycan binding were diverse, especially residue 189 that was essential for the sialic acid binding (Dormitzer *et al.* 2002b). Bat LZHP2 P[3] VP8* possessed 189 cysteine (C189), while

all the other tested P[3] VP8*s had tyrosine (Y189) (Fig. 6). V144 and T191 in bat LZHP2 P[3] VP8* are the same as that of bat-origin human M2-102, while human HCR3A, 12,638, and dog RV 198–95 P[3] VP8*s possessed S144 and A191. Residues R101, T146, Y155, G187, Y188, S190 are relatively conserved in all these P[3] VP8*s except H155 in human HCR3A.

Structural Analysis of the Glycan Binding Site of P[3] VP8*s

The homology model of bat P[3] VP8* was constructed based on the P[3] RRV crystal structure (PDB ID: 1KQR) by SWISS-MODEL. The structural superimposition showed that bat P[3] VP8* model presented typical galectin-like conformation, but it is quite different to RRV P[3] VP8* with the root mean square deviations (RMSD) values of 1.256 (Fig. 7A). Y189 in RRV P[3] formed hydrogen bonds with sialic acid, while C189 would lost the interaction (Fig. 7A), which may affect the ligand recognition. V144 and T191 may influence the interactions via the loop conformation, which still need further study to clarify. The surface presentation exhibited that the putative
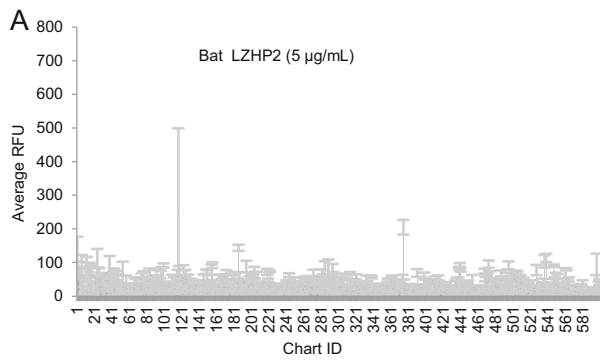
A — Bat LZHP2 (5 µg/mL)

Chart ID	Bat LZHP2 (5 µg/mL)	Average RFU	StDev	% CV
117	Gala1-3Galb1-4Glc-Sp10	257	242	94
375	GalNAcb1-4GlcNAcb1-2Mana1-6(GalNAcb1-4GlcNAcb1-2Mana1-3)Manb1-4GlcNAcb1-4GlcNAc-Sp12	205	22	11
186	GlcNAcb1-4-MDPLys	144	9	6
1	Gala-Sp8	114	62	55
539	Galb1-4GlcNAcb1-3Galb1-4GlcNAcb1-3Galb1-4GlcNAcb1-2Mana1-6(Galb1-4GlcNAcb1-3Galb1-4GlcNAcb1-3Galb1-4GlcNAcb1-2Mana1-3)Manb1-4GlcNAcb1-4GlcNAcb-Sp12	114	12	11
537	GlcNAcb1-3Galb1-4GlcNAcb1-3Galb1-4GlcNAcb1-2Mana1-6(GlcNAcb1-3Galb1-4GlcNAcb1-3Galb1-4GlcNAcb1-2Mana1-3)Manb1-4GlcNAcb1-4GlcNAcb-Sp12	104	19	18
473	Neu5Aca2-3Galb1-4GlcNAcb1-2Mana-Sp0	95	11	11
156	Galb1-4(6S)Glcb-Sp8	92	8	9
440	(6S)Galb1-3(6S)GlcNAc-Sp0	92	7	7
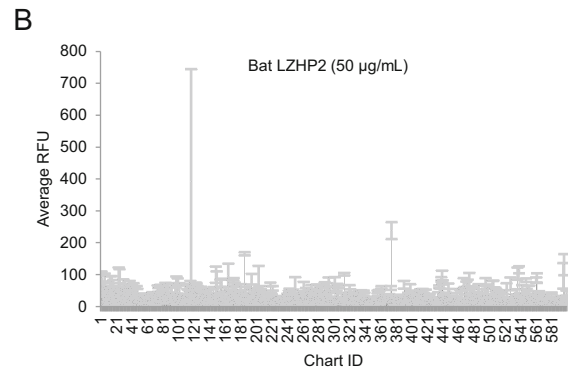
B — Bat LZHP2 (50 µg/mL)

Chart ID	Bat LZHP2 (50 µg/mL)	Average RFU	StDev	% CV
117	Gala1-3Galb1-4Glc-Sp10	393	352	90
375	GalNAcb1-4GlcNAcb1-2Mana1-6(GalNAcb1-4GlcNAcb1-2Mana1-3)Manb1-4GlcNAcb1-4GlcNAc-Sp12	238	27	11
186	GlcNAcb1-4-MDPLys	165	5	3
597	Neu5Aca2-3Galb1-4GlcNAcb1-3Galb1-4GlcNAcb1-3Galb1-4GlcNAcb1-2Mana1-6(Neu5Aca2-3Galb1-4GlcNAcb1-3Galb1-4GlcNAcb1-3Galb1-4GlcNAcb1-2Mana1-3)Manb1-4GlcNAcb1-4GlcNAcb-Sp12	131	33	25
539	Galb1-4GlcNAcb1-3Galb1-4GlcNAcb1-3Galb1-4GlcNAcb1-2Mana1-6(Galb1-4GlcNAcb1-3Galb1-4GlcNAcb1-3Galb1-4GlcNAcb1-2Mana1-3)Manb1-4GlcNAcb1-4GlcNAcb-Sp12	115	11	9
1	Gala-Sp8	103	6	6
537	GlcNAcb1-3Galb1-4GlcNAcb1-3Galb1-4GlcNAcb1-2Mana1-6(GlcNAcb1-3Galb1-4GlcNAcb1-3Galb1-4GlcNAcb1-2Mana1-3)Manb1-4GlcNAcb1-4GlcNAcb-Sp12	103	19	19
314	Mana1-2Mana1-6(Mana1-2Mana1-3)Mana1-6(Mana1-2Mana1-3)Mana-Sp9	101	4	4
149	Galb1-3GlcNAcb-Sp0	99	26	26
165	Galb1-4GlcNAcb1-3Galb1-4Glcb-Sp8	97	38	39
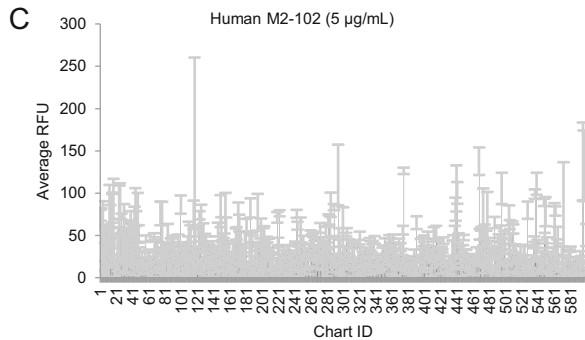
C — Human M2-102 (5 µg/mL)

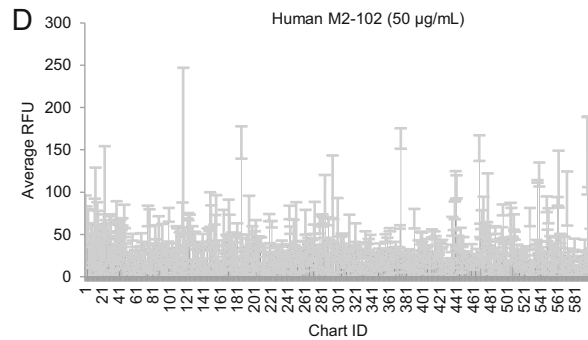| Chart ID	human M2-102 (5 µg/mL)	Average RFU	StDev	% CV
117	Gala1-3Galb1-4Glc-Sp10	139	121	87
468	Fuca1-2Galb1-4(Fuca1-3)GlcNAcb1-2Mana1-6(Fuca1-2Galb1-4(Fuca1-3)GlcNAcb1-2Mana1-3)Manb1-4GlcNAcb1-4(Fuca1-6)GlcNAcb-Sp24	138	16	12
596	Neu5Aca2-6Galb1-4GlcNAcb1-3Galb1-4GlcNAcb1-3Galb1-4GlcNAcb1-2Mana1-6(Neu5Aca2-6Galb1-4GlcNAcb1-3Galb1-4GlcNAcb1-3Galb1-4GlcNAcb1-2Mana1-3)Manb1-4GlcNAcb1-4GlcNAcb-Sp12	138	46	33
597	Neu5Aca2-3Galb1-4GlcNAcb1-3Galb1-4GlcNAcb1-2Mana1-6(Neu5Aca2-3Galb1-4GlcNAcb1-3Galb1-4GlcNAcb1-3Galb1-4GlcNAcb1-2Mana1-3)Manb1-4GlcNAcb1-4GlcNAcb-Sp12	132	42	32
375	GalNAcb1-4GlcNAcb1-2Mana1-6(GalNAcb1-4GlcNAcb1-2Mana1-3)Manb1-4GlcNAcb1-4GlcNAc-Sp12	127	4	3
294	4S(3S)Galb1-4GlcNAcb-Sp0	122	36	30
539	Galb1-4GlcNAcb1-3Galb1-4GlcNAcb1-3Galb1-4GlcNAcb1-2Mana1-6(Galb1-4GlcNAcb1-3Galb1-4GlcNAcb1-3Galb1-4GlcNAcb1-2Mana1-3)Manb1-4GlcNAcb1-4GlcNAcb-Sp12	111	13	12
440	(6S)Galb1-3(6S)GlcNAc-Sp0	106	27	26
496	Fuca1-2(6S)Galb1-3(6S)GlcNAcb-Sp0	106	19	18
441	Fuca1-2Galb1-4 GlcNAcb1-2Mana1-6(Fuca1-2Galb1-4GlcNAcb1-2(Fuca1-2Galb1-4GlcNAcb1-4)Mana1-3)Manb1-4GlcNAcb1-4GlcNAcb-Sp12	100	13	13

D — Human M2-102 (50 µg/mL)

Chart ID	Human M2-102 (50 µg/mL)	Average RFU	StDev	% CV
375	GalNAcb1-4GlcNAcb1-2Mana1-6(GalNAcb1-4GlcNAcb1-2Mana1-3)Manb1-4GlcNAcb1-4GlcNAc-Sp12	163	12	7
186	GlcNAcb1-4-MDPLys	159	19	12
468	Fuca1-2Galb1-4(Fuca1-3)GlcNAcb1-2Mana1-6(Fuca1-2Galb1-4(Fuca1-3)GlcNAcb1-2Mana1-3)Manb1-4GlcNAcb1-4(Fuca1-6)GlcNAcb-Sp24	152	15	10
597	Neu5Aca2-3Galb1-4GlcNAcb1-3Galb1-4GlcNAcb1-2Mana1-6(Neu5Aca2-3Galb1-4GlcNAcb1-3Galb1-4GlcNAcb1-3Galb1-4GlcNAcb1-2Mana1-3)Manb1-4GlcNAcb1-4GlcNAcb-Sp12	148	42	28
596	Neu5Aca2-6Galb1-4GlcNAcb1-3Galb1-4GlcNAcb1-2Mana1-6(Neu5Aca2-6Galb1-4GlcNAcb1-3Galb1-4GlcNAcb1-2Mana1-3)Manb1-4GlcNAcb1-4GlcNAcb-Sp12	143	46	32
539	Galb1-4GlcNAcb1-3Galb1-4GlcNAcb1-3Galb1-4GlcNAcb1-2Mana1-6(Galb1-4GlcNAcb1-3Galb1-4GlcNAcb1-3Galb1-4GlcNAcb1-2Mana1-3)Manb1-4GlcNAcb1-4GlcNAcb-Sp12	121	14	12
562	Galb1-4GlcNAcb1-3Galb1-4GlcNAcb1-6(Galb1-3GlcNAcb1-3Galb1-4GlcNAb1-2)Mana1-6(Galb1-3GlcNAcb1-3Galb1-4GlcNAcb1-2Mana1-3)Manb1-4GlcNAcb1-4(Fuca1-6)GlcNAcb-Sp24	115	34	29
537	GlcNAcb1-3Galb1-4GlcNAcb1-3Galb1-4GlcNAcb1-2Mana1-6(GlcNAcb1-3Galb1-4GlcNAcb1-3Galb1-4GlcNAcb1-2Mana1-3)Manb1-4GlcNAcb1-4GlcNAcb-Sp12	113	2	1
440	(6S)Galb1-3(6S)GlcNAc-Sp0	108	17	16
294	4S(3S)Galb1-4GlcNAcb-Sp0	106	37	35

◄ **Fig. 3** Graphical representation of P[3] VP8* (bat LZHP2 (up panel), human M2-102 (bottom panel)) VP8* at (**A/C**) 5 μg/mL, and (**B/D**) 50 μg/mL binding to the array of 600 glycans. Relative Fluorescent Units (RFU) correspond to the strength of binding to individual glycans. Binding specificity is shown in mean relative fluorescence units (RFU) of binding to n = 6 replicates of each glycan printed on the array and % coefficient of variation (%CV). The highest and lowest point from each set of 6 replicates has been removed so the average is of 4 values. The strength of binding at two concentrations is shown. Data for the top 10 of the glycans bound with highest intensity are listed in each table.

sialic acid binding site was discontinuous in the P[3] bat VP8* model (Fig. 7B). The electrostatic potential was also different with positive charge in P[3] bat VP8* model and negative charge in P[3] RRV VP8* (Fig. 7C).

Discussion

Many rotavirus genotypes can infect different species and species-specific RV strains are frequently identified (Papp *et al.* 2013). The zoonotic potential has led to the increased burden of RV control and prevention (Doro *et al.* 2015). The glycan binding specificity of different virus strains are vital for understanding the host infection and tropism (Ramani *et al.* 2016). VP8*, located at the distal terminal of the VP4 spike, was involved in the glycan recognition and played an important role in the virus attachment

(Huang *et al.* 2012; Ramani *et al.* 2016). Bats are recognized as the reservoir of many viruses, including the life-threatening Ebola virus, SARS, influenza virus. Rotaviruses in bats were identified by several studies (Esona *et al.* 2010; He *et al.* 2013, 2017). P[3] RVs are also found in cats/dogs and some feline/canine-like RVA strains are identified to infect humans sporadically (Tsugawa and Hoshino 2008). The glycan specificity and molecular mechanism of the cross-species transmission is important for understanding the virus prevalence. Here, we delineated the functional features of P[3] RV VP8*s of different species.

Bat LZHP2 P[3] VP8* showed no hemagglutination to all the erythrocytes tested, while other VP8* hemagglutinated the cells, indicating that bat LZHP2 P[3] VP8* probably do not interact with classical ligands that were recognized by Rhesus P[3] RV (Dormitzer *et al.* 2002a). Glycan binding assay verified that human HCR3A, 12,638, and dog RV198-95 P[3] VP8* bound to glycans with sialic acid while bat P[3] VP8* did not. Human M2-102 hemagglutinated the red blood cells, while showed no obvious binding to the glycans with sialic acid, providing more evidence that human M2-102 was originated from bat P[3] RVs. Human HCR3A and dog RV198-95 P[3] exhibited similar binding to both Neu5Acα2-3Gal and Neu5Acα2-6Gal, indicating that these P[3] RV bound sialic acid irrespective of the α2-3 or α2-6 linkage and
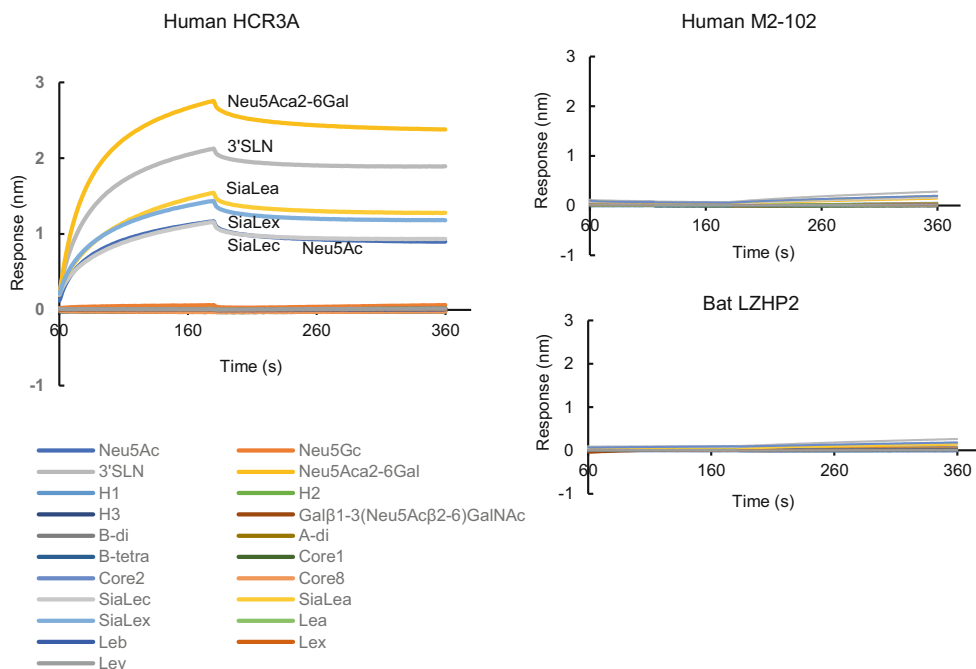
Fig. 4 Biolayer interometry (BLI) analysis. PAA-biotin labeled oligosaccharides, Neu5Ac, Neu5Gc, Neu5Acα2-3Galβ1-4GlcNA-(3'SLN), Neu5Acα2-6Gal, H1, H2, H3, Neu5Acβ2-6(Galβ1-3)Gal-NAc, B disaccharide, A disaccharide, B tetrasaccharide, core1, core2, core8, siaLea, siaLex, siaLec, lea, leb, lex, ley were loaded on the biosensor at 10 μg/mL. Human HCR3A, M2-102, and bat LZHP2 P[3] VP8* proteins were diluted at 10 μmol/L and applied to the association and dissociation procedures. The glycan binding data was analyzed by the Octet analyzing software.
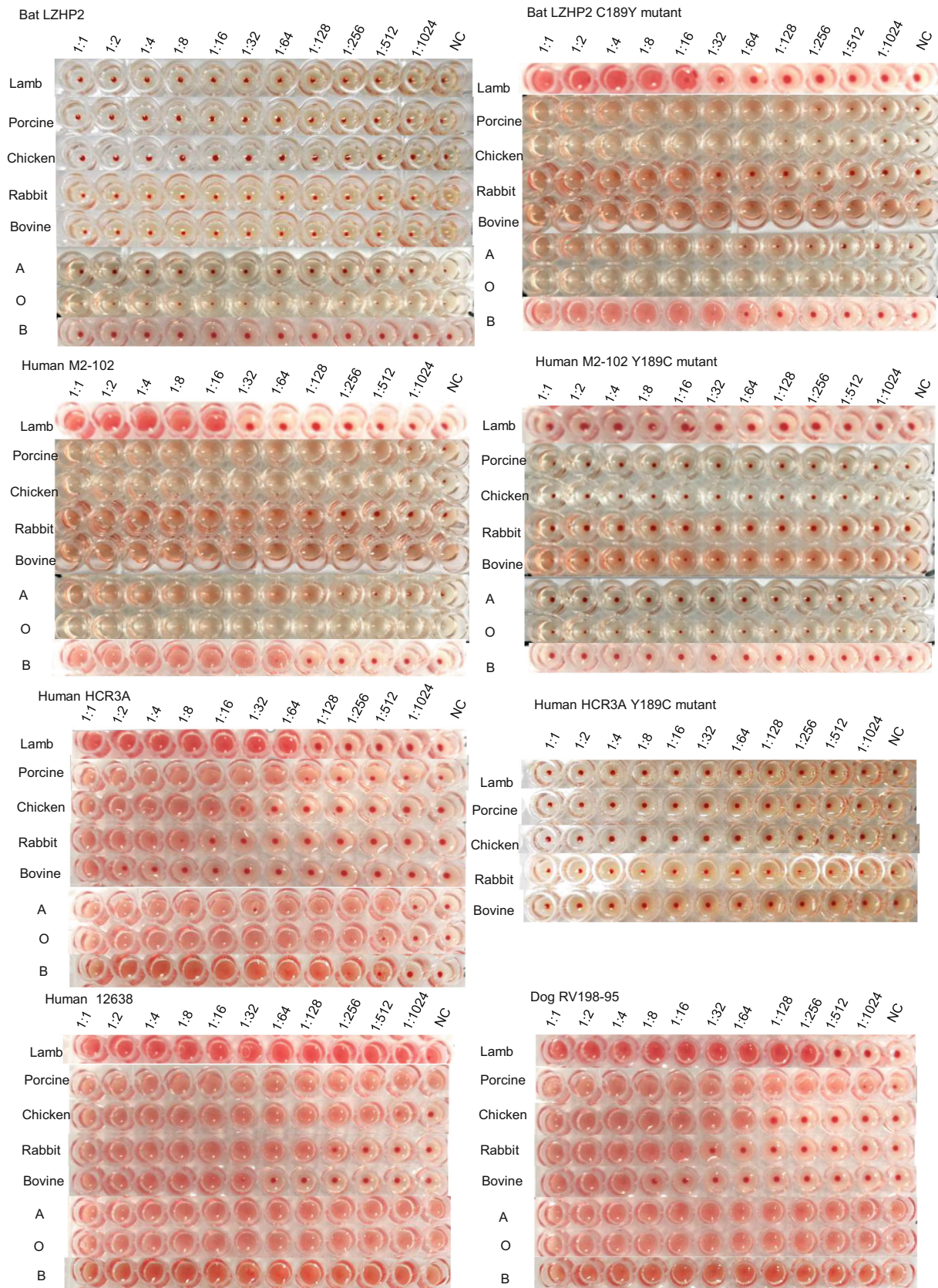
Fig. 5 The hemagglutination assay of P[3] RV VP8*s. Red blood cells of chicken, porcine, rabbit, bovine, human A, B, O were used in the assay. The protein at 2 mg/mL was diluted serially with PBS as shown. PBS buffer was used as the negative control (NC).

Fig. 6 VP8* protein sequences of different P[3] strains were aligned using DNAMAN. The residues involved in the ligand binding were colored red. The amino acids that are different between bat and human/dog were presented in green. H155 in human HCR3A VP8* was colored blue. Residue C189 was colored yellow. GeneBank numbers of the sequences are: bat LZHP2 (KX814943), human M2-102 (KU597745), human HCR3A (EU708904), human 12,638 (LC340022), dog RV198-95 (HQ661137).
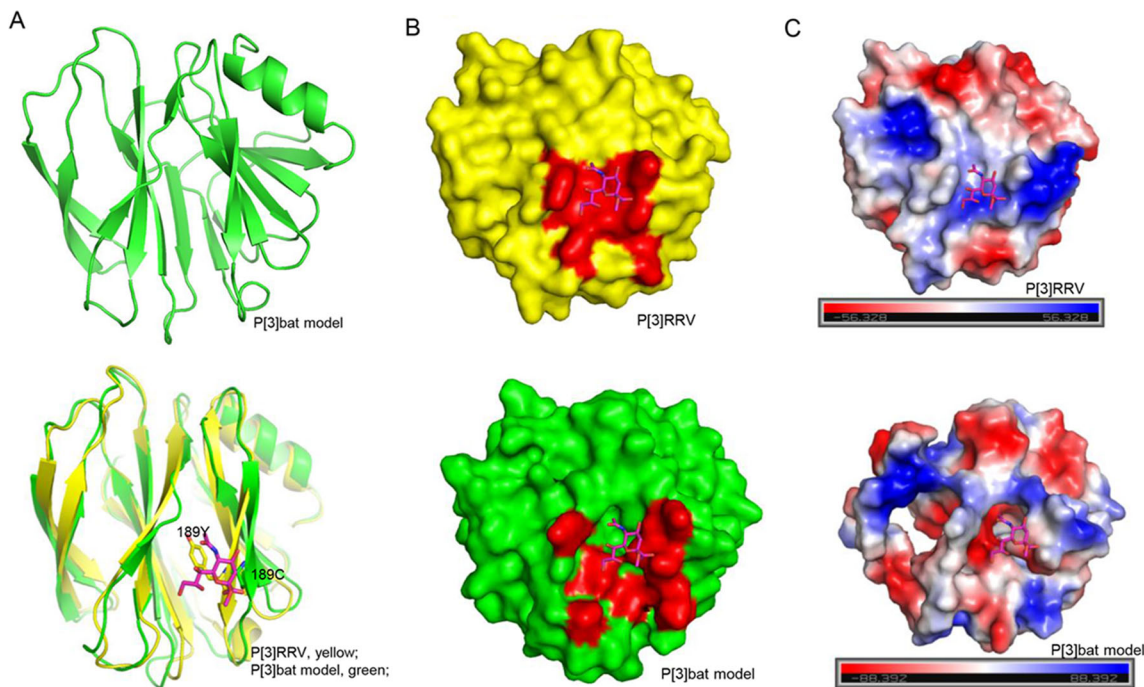
Fig. 7 Structural analysis of P[3] VP8*s. **A** Bat P[3] VP8* model was constructed using the SWISS-MODEL. Bat P[3] VP8* was superimposed to P[3] RRV VP8*s. VP8* was shown as cartoon. Residue 189 Y/C was emphasized using stick. Sialic acid was shown as stick. **B** P[3] RRV and P[3] bat VP8*s were shown as surface. The glycan binding site and putative glycan binding pocket were colored red. **C** The electrostatic potential presentation of P[3] RRV and P[3] bat VP8*s. Red and blue indicate the positive and negative charge, respectively.
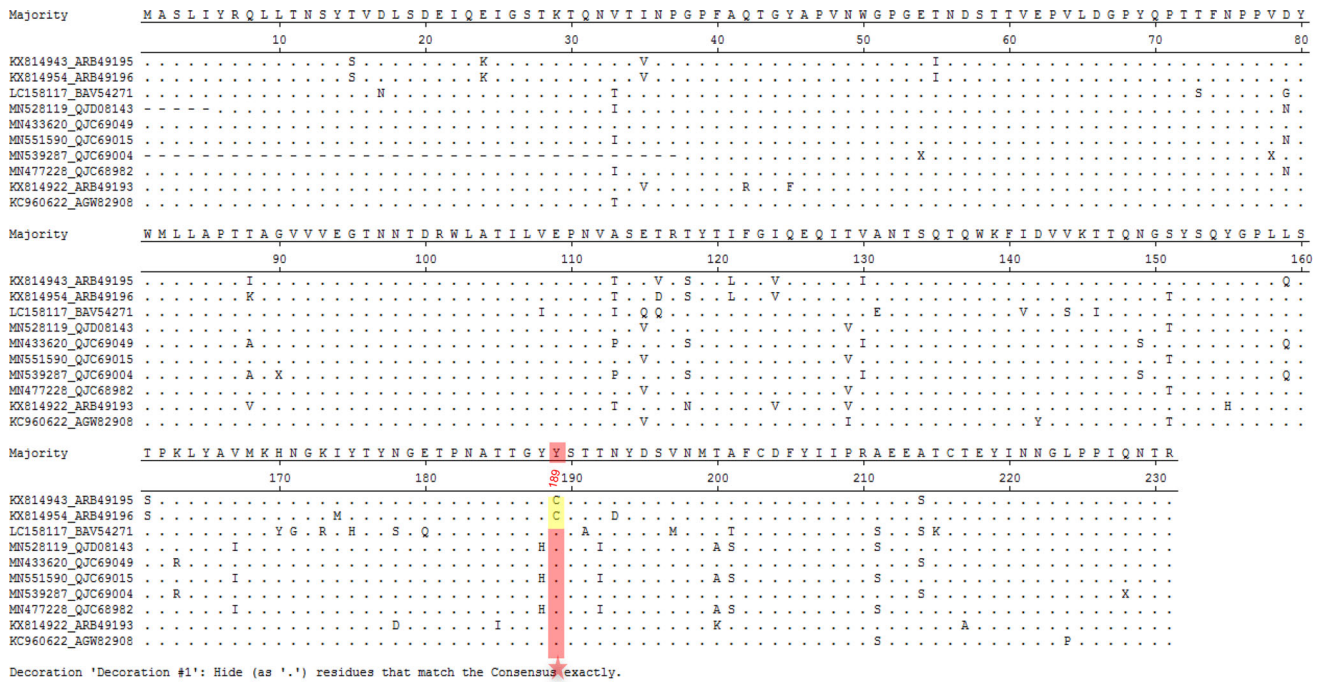
Fig. 8 Sequence alignment of ten bat P[3] RV VP8* protein sequences. The sequence alignment was done with MegAlign. Residue 189 was pointed with red star. 189C was colored yellow and 189Y was colored red. GeneBank numbers of the sequences are as following: LZHP2 (KX814943), YSSK5 (KX814954), LUS12-14 (LC158117), GKS-894 (MN528119), BB89-15 (433,620), GKS-94 (MN551590), BR89-60 (MN539287), GKS-954 (MN477228), BSTM70 (KX814922), MSLH14 (KC960622).

possessed the potential of cross-species transmission. These results demonstrated that different P[3] VP8*s had various hemagglutination ability and glycan binding specificity. Bat P[3] VP8*s displayed no binding to sialic acid and probably could not infect human, while human/-dog origin P[3] VP8*s bound sialic acid and could infect both human and animals.

Sequence alignment showed that several amino acids were different between bat LZHP2 and human RV VP8*s, including the residue 189. Bat LZHP2 C189Y mutant obtained the ability of hemagglutination while human P[3] Y189C mutant had no hemagglutination, implying that residue 189 was one of the key residues for the ligand recognition and the C189Y alteration in M2-102 RV probably facilitate the sporadic bat-origin RV infection in human. Meanwhile, other amino acids, including residue 144, 155, and 191 may contribute to the different glycan binding capacity of P[3] VP8*.

The structural analysis revealed that the putative glycan binding site in bat P[3] VP8* model was quite different to that in the P[3] RRV VP8*, which partially explained that bat VP8* did not bind sialic acid glycans. These indicated that species barrier probably existed for bat LZHP2 P[3] RVs. Bat LZHP2 P[3] RV could not transmit to humans at present but may infect human sporadically with the C189Y alteration. Analysis of all the reported bat P[3] RV VP8* sequences showed that bat LZHP2 and YSSK5 (He *et al.*

2017) possessed 189C, while other 8 strains contained 189Y (Fig. 8), implying that some bat P[3] RV strains may have the potential to infect human like the M2-102 strain. Therefore, the consistent surveillance of bat and animal RVs is needed.

Author contribution ZD, DL, and XS designed the experiments; MXW, DL, TM, and LP performed the protein expression and the glycan binding assay. MXW, MWW, QZ and HW carried out the hemagglutination assay. XS performed the biolayer interferometry assay and the structural analysis. XS and DL analyzed the data and constructed the figures. XS wrote the original draft of the manuscript. DL, ZD and XS revised the manuscript. All authors reviewed the manuscript and provided inputs.

Compliance with EthicalStandards

Conflict of interest All authors declare no potential conflict of interest.

References

Banyai K, Kemenesi G, Budinski I, Foldes F, Zana B, Marton S, Varga-Kugler R, Oldal M, Kurucz K, Jakab F (2017) Candidate new rotavirus species in Schreiber's bats, Serbia. Infect Genet Evol 48:19–26

Blanchard H, Yu X, Coulson BS, von Itzstein M (2007) Insight into host cell carbohydrate-recognition by human and porcine rotavirus from crystal structures of the virion spike associated carbohydrate-binding domain (VP8*). J Mol Biol 367:1215–1226

Cholleti SR, Agravat S, Morris T, Saltz JH, Song X, Cummings RD, Smith DF (2012) Automated motif discovery from glycan array data. OMICS 16:497–512

Ciarlet M, Estes MK (1999) Human and most animal rotavirus strains do not require the presence of sialic acid on the cell surface for efficient infectivity. J Gen Virol 80:943–948

Dong H, Qian Y, Nong Y, Zhang Y, Mo Z, Li R (2016) Genomic characterization of an unusual human G3P[3] rotavirus with multiple cross-species reassortment. Bing Du Xue Bao 32:129–140

Dormitzer PR, Sun ZY, Blixt O, Paulson JC, Wagner G, Harrison SC (2002a) Specificity and affinity of sialic acid binding by the rhesus rotavirus VP8* core. J Virol 76:10512–10517

Dormitzer PR, Sun ZY, Wagner G, Harrison SC (2002b) The rhesus rotavirus VP4 sialic acid binding domain has a galectin fold with a novel carbohydrate binding site. EMBO J 21:885–897

Doro R, Farkas SL, Martella V, Banyai K (2015) Zoonotic transmission of rotavirus: surveillance and control. Expert Rev Anti Infect Ther 13:1337–1350

Esona MD, Mijatovic-Rustempasic S, Conrardy C, Tong S, Kuzmin IV, Agwanda B, Breiman RF, Banyai K, Niezgoda M, Rupprecht CE, Gentsch JR, Bowen MD (2010) Reassortant group A rotavirus from straw-colored fruit bat (Eidolon helvum). Emerg Infect Dis 16:1844–1852

Estes MK (2013) Greenberg HB rotaviruses. In: Knipe DM, Howley PM et al (eds) Fields virology, 6th edn. Wolters Kluwer Health/ Lippincott Williams & Wilkins, Philadelphia, pp 1347–1401

Fiore L, Greenberg HB, Mackow ER (1991) The VP8 fragment of VP4 is the rhesus rotavirus hemagglutinin. Virology 181:553–563

He B, Huang X, Zhang F, Tan W, Matthijnssens J, Qin S, Xu L, Zhao Z, Yang L, Wang Q, Hu T, Bao X, Wu J, Tu C (2017) Group a rotaviruses in chinese bats: genetic composition, serology, and evidence for bat-to-human transmission and reassortment. J Virol 91.e02493

He B, Yang F, Yang W, Zhang Y, Feng Y, Zhou J, Xie J, Feng Y, Bao X, Guo H, Li Y, Xia L, Li N, Matthijnssens J, Zhang H, Tu C (2013) Characterization of a novel G3P[3] rotavirus isolated from a lesser horseshoe bat: a distant relative of feline/canine rotaviruses. J Virol 87:12357–12366

Huang P, Xia M, Tan M, Zhong W, Wei C, Wang L, Morrow A, Jiang X (2012) Spike protein VP8* of human rotavirus recognizes histo-blood group antigens in a type-specific manner. J Virol 86:4833–4843

Isa P, Arias CF, Lopez S (2006) Role of sialic acids in rotavirus infection. Glycoconj J 23:27–37

Komoto S, Tacharoenmuang R, Guntapong R, Upachai S, Singchai P, Ide T, Fukuda S, Hatazawa R, Sutthiwarakom K, Kongjorn S, Onvimala N, Luechakham T, Sriwanthana B, Murata T, Uppapong B, Taniguchi K (2020) Genomic characterization of a novel G3P[10] rotavirus strain from a diarrheic child in Thailand: Evidence for bat-to-human zoonotic transmission. Infect Genet Evol 87:104667

Ma X, Li DD, Sun XM, Guo YQ, Xiang JY, Wang WH, Zhang LX, Gu QJ, Duan ZJ (2015) Binding patterns of rotavirus genotypes P[4], P[6], and P[8] in China with histo-blood group antigens. PLoS One 10:e0134584

Matthijnssens J, Ciarlet M, McDonald SM, Attoui H, Banyai K, Brister JR, Buesa J, Esona MD, Estes MK, Gentsch JR, Iturriza-Gomara M, Johne R, Kirkwood CD, Martella V, Mertens PP, Nakagomi O, Parreno V, Rahman M, Ruggeri FM, Saif LJ, Santos N, Steyer A, Taniguchi K, Patton JT, Desselberger U, Van Ranst M (2011) Uniformity of rotavirus strain nomenclature proposed by the rotavirus classification working group (RCWG). Arch Virol 156:1397–1413

Nyaga MM, Tan Y, Seheri ML, Halpin RA, Akopov A, Stucker KM, Fedorova NB, Shrivastava S, Duncan Steele A, Mwenda JM, Pickett BE, Das SR, Jeffrey Mphahlele M (2018) Whole-genome sequencing and analyses identify high genetic heterogeneity, diversity and endemicity of rotavirus genotype P[6] strains circulating in Africa. Infect Genet Evol 63:79–88

Okitsu S, Hikita T, Thongprachum A, Khamrin P, Takanashi S, Hayakawa S, Maneekarn N, Ushijima H (2018) Detection and molecular characterization of two rare G8P[14] and G3P[3] rotavirus strains collected from children with acute gastroenteritis in Japan. Infect Genet Evol 62:95–108

Papp H, Laszlo B, Jakab F, Ganesh B, De Grazia S, Matthijnssens J, Ciarlet M, Martella V, Banyai K (2013) Review of group A rotavirus strains reported in swine and cattle. Vet Microbiol 165:190–199

Ramani S, Hu L, Venkataram Prasad BV, Estes MK (2016) Diversity in rotavirus-host glycan interactions: a "sweet" spectrum. Cell Mol Gastroenterol Hepatol 2:263–273

Sasaki M, Orba Y, Sasaki S, Gonzalez G, Ishii A, Hang'ombe BM, Mweene AS, Ito K, Sawa H (2016) Multi-reassortant G3P[3] group A rotavirus in a horseshoe bat in Zambia. J Gen Virol 97:2488–2493

Sun X, Dang L, Li D, Qi J, Wang M, Chai W, Zhang Q, Wang H, Bai R, Tan M, Duan Z (2020) Structural basis of glycan recognition in globally predominant human p[8] rotavirus. Virol Sin 35:156–170

Sun X, Li D, Qi J, Chai W, Wang L, Wang L, Peng R, Wang H, Zhang Q, Pang L, Kong X, Wang H, Jin M, Gao GF, Duan Z (2018) Glycan binding specificity and mechanism of human and porcine P[6]/P[19] rotavirus VP8*s. J Virol 92:e00538–18

Tsugawa T, Hoshino Y (2008) Whole genome sequence and phylogenetic analyses reveal human rotavirus G3P[3] strains Ro1845 and HCR3A are examples of direct virion transmission of canine/feline rotaviruses to humans. Virology 380:344–353